Nuclear Materials and Energy 46 (2026) 102059

Contents lists available at ScienceDirect

Nuclear Materials and Energy

journal homepage: www.elsevier.com/locate/nme

Depth-resolved deuterium retention profiles in displacement-damaged tungsten measured via picosecond-laser-induced ablation quadrupole mass spectrometry ☆

C. Kawan [a,b,*], S. Brezinsek [a,b], E. Wüst [a,b], T. Dittmar [a], T. Schwarz-Selinger [c], M. Rasinski [a], S. Möller [d], L. Gao [a], Ch. Linsmeier [a]

[a] Forschungszentrum Jülich GmbH, Institute for Fusion Energy and Nuclear Waste Management - Plasma Physics, Partner of the Trilateral Euregio Cluster (TEC), 52425 Jülich, Germany

[b] Mathematisch- Naturwissenschaftliche Fakultät, Heinrich-Heine-Universität Düsseldorf, 40225 Düsseldorf, Germany

[c] Max–Planck-Institut für Plasmaphysik, Boltzmannstrasse 2, 85748 Garching, Germany

[d] Forschungszentrum Jülich GmbH, Institute of Energy Materials and Devices, Materials Synthesis and Processing (IMD-2), 52425 Jülich, Germany

ARTICLE INFO

Keywords:
LIA-QMS
Laser-induced ablation quadrupole mass spectrometry
Deuterium retention
In-situ D retention analysis
Fuel retention
Laser-material-interaction

ABSTRACT

Tungsten (W) is the most promising plasma-facing material candidate for future deuterium–tritium (D–T) fusion reactors due to its favorable properties, such as low sputtering yield, low chemical reactivity, high melting point, and low intrinsic fuel retention. However, highly energetic neutrons from DT fusion reactions can cause displacement damage in the W lattice and enhance fuel retention. This affects the tritium cycle requirements and nuclear safety, as a tritium inventory builds up in the vessel. Therefore, diagnostics are required to quantify the D and T content in-situ in the plasma-facing and structural materials. Laser-induced Ablation Quadrupole Mass Spectrometry (LIA-QMS) is a promising method for quantifying fuel content with good spatial and depth resolution. LIA-QMS can be simultaneously applied with Laser-induced Breakdown Spectroscopy (LIBS). Combining both techniques provides the high depth resolution of LIBS with the quantification capabilities of LIA-QMS. This study compares D depth profiles recorded with pico-second LIA-QMS with Nuclear Reaction Analysis (NRA) with ^{3}He beam on a displacement-damaged W sample. The comparison reveals the depth profiling capabilities, strengths, and weaknesses of LIA-QMS using picosecond lasers. A set of similarly self-damaged (10.8 MeV W^{3+} irradiated) ITER-grade W samples from PLANSEE was gently loaded with D in a low-temperature plasma at 370 K. The D concentration was varied by subsequent annealing of the samples at different temperatures in a vacuum after the D decoration. The ratio between D_2 and HD, both contributing to the total D content, increases from 1:1 to 1:5, starting at the surface and extending to 4 μm, with increasing depth. LIA-QMS shows a similarly high sensitivity (<0.05 at% D at a 15 nm average ablation rate (AAR)) as NRA (around 150-400 nm resolution). ps-LIA-QMS can be calibrated via a known amount of reference gas injections and deviates from the NRA results by a factor of 1.7 across all samples, which also includes non-volatile species. The laser-induced crater surface stays relatively flat for up to 4 μm until surface structures start dominating the crater's surface under the given laser parameters. μ-NRA in and around the craters shows complete removal of D inside the laser crater. Thermal effects due to the ps-pulses within the crater floor are indicated, but could not be quantified yet. In conclusion, this study shows a good agreement between ps-LIA-QMS, a potential in-situ method, and the reference ex-situ method NRA for D quantification. This paves the way for studies to investigate open questions about particle–wall interactions during the ablation process.

☆ This article is part of a Special issue entitled: 'PFMC-20' published in Nuclear Materials and Energy.

* Corresponding author at: Forschungszentrum Jülich GmbH, Institute for Fusion Energy and Nuclear Waste Management - Plasma Physics, Partner of the Trilateral Euregio Cluster (TEC), 52425 Jülich, Germany.
E-mail address: c.kawan@fz-juelich.de (C. Kawan).

https://doi.org/10.1016/j.nme.2026.102059
Received 27 July 2025; Received in revised form 29 December 2025; Accepted 8 January 2026
Available online 9 January 2026

1. Introduction

The hydrogen isotopes deuterium (D) and tritium (T) are the most promising fuel gases for fusion reactors due to their relatively large cross section and availability. These isotopes have been employed in experimental devices, such as the Joint European Torus (JET) [1], to investigate burning-plasma behavior and confinement improvements during operation with the metallic first wall. Although DT fusion exhibits superior performance compared to other fusion reactions, the use of T poses significant challenges. While D has a natural occurrence of approximately ~0.015% in water, T has no natural occurrence and must be bred in dedicated breeding blankets within the fusion device, as it will be tested in ITER [2]. Therefore, efficient fuel usage is crucial for a closed fuel cycle and economical operation. Furthermore, the radioactivity of T, with a half-life of approximately 12.3 years, significantly impacts reactor design and operation, necessitating compliance with radiation safety requirements. Given these properties, a closed fuel cycle is essential for efficient, safe, and long-term operation of a reactor. The closure of the fuel cycle is closely linked to fuel retention in the first-wall materials, which serve as the primary interaction area, and to breeding efficiency.

Tungsten (W) is envisioned as the primary material for the first wall of fusion devices due to its high melting point, high thermal conductivity, low activation potential, minimal chemical interactions, and favorable fuel retention properties. However, the microstructure of W undergoes significant changes during operation due to different types of particles, e.g., He ash and seed species such as Ne. The high flux of energetic plasma particles in the eV to keV range impinging on the surface causes, on the one hand, material erosion and, on the other hand, irradiation damage on a micrometer scale, increasing the likelihood of incoming fuel atoms becoming trapped and thereby enhancing retention [3]. However, the primary contributor to irradiation damage inside the reactor is expected to be the 14 MeV high-energy neutrons generated by the DT fusion process, which can penetrate deep into the material [4]. This induces displacement damage much deeper than the penetration depth of plasma particles, thereby creating a potential retention volume, e.g., via voids. Collision cascades mainly drive the damage created by neutrons and cause degradation of mechanical properties to an extent that plasma particles or eroded material do not [5]. While neutron irradiation causes activation and its high penetration depth leads to a homogeneous damaging pattern, proton irradiation, used to mimic the damage of neutrons, creates blisters under certain conditions in the depth where the Bragg peak occurs and is limited on the micrometer scale [6,7]. Synergistic effects among neutrons, plasma ions, impurities, and wall temperatures also alter the microstructure and retention properties, unlike those of single damage sources. The observed types of lattice damage and synergistic effects are discussed in [3]. The fuel retention shows a strong dependence on the damage dose, quantified in displacements per atom (dpa), increasing rapidly at low damage doses and saturating at around 0.1 dpa. For ITER, the maximum dose is expected to be 0.25 dpa at the end of lifetime [8,9].

For these reasons, diagnostics are needed to investigate the T stored in the first-wall components at certain time intervals to monitor the in-vessel fuel inventory, before component replacement, and finally during decommissioning. One common diagnostic to quantify hydrogen isotope retention is Nuclear Reaction Analysis (NRA), which uses nuclear reactions to analyze the composition of the surface and at depths of a few micrometers [10]. Although NRA is depth-resolved, non-destructive, and highly sensitive, it is not applicable to fusion devices as an in-situ technique due to the extensive and costly facilities required for ion acceleration, the remnant magnetic fields that deflect the ion beam, and the limited analyzable depth. As an alternative, laser-based diagnostics are promising tools for determining the T content in-situ in future fusion devices. In-situ experiments with laser-induced desorption quadrupole mass spectrometry (LID-QMS) at JET proved the extremely high sensitivity of mass spectrometry after laser-induced desorption of hydrogen isotopes [11]. This technique allows fast analysis of the total amount of retained D and T but offers no specific depth resolution. Another technique, which is already implemented in several devices as an in-situ technique, is laser-induced breakdown spectroscopy (LIBS) [12,13], for example, in JET [14]. LIBS is a depth-resolved method that uses short-pulse laser ablation to create a plasma, whose optical spectrum is observed with a spectrometer to determine the composition of the plasma formed. Direct quantification requires separating the line emission from deuterium and tritium, which is challenging due to line broadening and photon-to-particle conversion. Normalization against reference samples, or so-called calibration-free LIBS, might be used for quantification. As a combination of "the best of both worlds" for hydrogen quantification and good depth resolution, laser-induced ablation quadrupole mass spectrometry was developed, using residual gas analysis of the laser-ablated material with a quadrupole mass spectrometer. The first studies for LIA-QMS have already been carried out for carbon (C), with promising results in terms of sensitivity and depth resolution [15]. LIA-QMS now needs to be adapted to W and other fusion-relevant materials with low fuel content to account for the different properties of chemical compounds, their response to laser pulses, ablation behavior, and retention properties [16,17]. The interactions between the ablated plasma particles and the first wall materials need to be investigated, and depth profiling optimized. Since high-energy fusion neutrons at high fluence are not yet available, experiments with pre-damaged W are carried out using self-damaging or proton irradiation as a proxy for high-energy neutrons in the near-surface regions. In the following, the capabilities of LIA-QMS utilizing a picosecond laser for analyzing D retention in self-damaged W as a proxy for neutron irradiation and fuel retention are demonstrated. Additionally, the validation of ps-LIA-QMS against NRA, the reference method, is presented, and the potential for simultaneous and complementary measurements with LIBS is explored.

2. Methods

2.1. Sample preparation

To mimic the combined effects of plasma and neutron irradiation, two sets of four W samples were subjected to a self-ion irradiation and D decoration procedure by low-temperature plasma exposure at the Max Planck Institute for Plasma Physics (IPP) in Garching, Germany. Before exposure, all samples were recrystallized under UHV conditions ($<5 \times 10^{-9}$ mbar) at 2000 K for 3 min. As a result of this procedure, vacancies were eliminated and intrinsic hydrogen removed; hence, the structure within the samples was homogenized, which otherwise could lead to difficulties when evaluating the damage profile applied in the following step. Seven out of eight samples were self-irradiated with 10.8 MeV W^{3+} ions at room temperature, to a fluence of 1×10^{14} W/cm^2. The SRIM calculated damage profile is shown in Fig. 1 marking 1.2 μm as the expected damage and hence implantation depth of D. Subsequently, all samples were decorated with D by the plasma source (PlaQ) at 370 K, with an energy of 5 eV per D atom, for 50.5 h. Then, six out of eight samples were outgassed in the quartz tube of the thermal effusion spectroscopy (TESS) facility. Following an empty ramp to 1010 K without samples to determine the background, the samples were heated with a temperature ramp (3 K/min) to different maximum temperatures, as detailed in Table 1. During outgassing, the mass spectrometer at TESS was employed to acquire thermal desorption spectroscopy (TDS) data as a secondary reference measurement [18].

After the outgassing procedure, all samples were analyzed with a 1 mm × 1 mm ^{3}He beam at an impact energy of 2.4 MeV, at 5–10 locations with a 2–1 mm step width, to provide information on the lateral homogeneity of the D content. Eight different ^{3}He energies were used, ranging from 4.5 MeV to 500 keV, yielding a depth resolution of about 150–400 nm. To derive the most probable D depth profile and the total D content within the information depth of 7.2 micrometers,

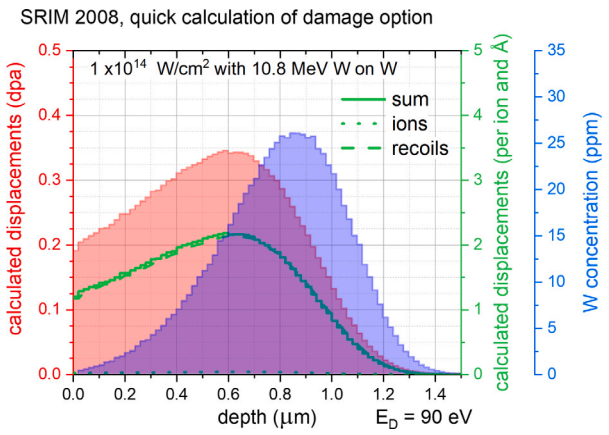

Fig. 1. Calculated displacements by the incoming 10.8 MeV W^{3+} ions, by the created recoils, and the sum of the two (green lines and axis). For the applied fluence of 1×10^{14} W/cm^2, this corresponds to the shown primary displacement damage (red line and axis) and the implanted W concentration (blue line and axis). (For interpretation of the references to color in this figure legend, the reader is referred to the web version of this article.)

all collected proton and alpha spectra were analyzed simultaneously with the NRADC software [19] together with SimNRA7.04 [20]. The 5% error in the cross-section determines the absolute accuracy, whereas the cross-section data from Wielunska et al. were used [21]. Following these NRA measurements, the samples were shipped to the Forschungszentrum Jülich (FZJ) for LIBS and LIA-QMS analysis. After the LIA-QMS measurements, μ-NRA was carried out to investigate the D content remaining in the crater floor. For the μ-NRA measurement, a ^{3}He beam with 2950 keV and a 100 µm spot size was used, irradiating for 4–6 min per spot for a total dose of 3 µC.

2.2. Experimental setup

The experimental setup for the LIA-QMS and LIBS measurements is illustrated in Fig. 2. All measurements were conducted at a constant room temperature of 293 K. Before sample installation, the analysis chamber was baked out at 433 K for 48 h to minimize outgassing from the steel chamber walls. The samples were mounted after nitrogen (N_2) flooding of the chamber to minimize the impact of air and other impurities. All samples were fixed on an x-, y-, ϕ-stage within the vacuum chamber, which had a volume of 0.3 m^3, and was operated at a base pressure of approximately 6×10^{-8} mbar. The position of the laser spot (around 700 µm in diameter) on the sample is controlled by the x and y coordinates; the angle phi describes the rotation about the manipulator's center axis and hence the incident angle of the laser beam on the sample. A turbo molecular pump was connected to the analysis chamber via a pneumatic valve, allowing the pump to be isolated shortly before the laser pulses. The valve to the pump stayed closed during the laser pulses to increase the sensitivity. For the QMS measurements, a Pfeiffer HiQuad QMG700 mass spectrometer was employed. Two calibration leaks were used to calibrate the deuterium (D) content: a Laco H_2 leak with a flow rate of 3.96×10^{-6} mbarl/s and a D_2 leak with a flow rate of 4.05×10^{-6} mbarl/s.

A Nd:YVO_4 laser (EKSPLA) operating at a wavelength of 355 nm and a pulse duration of 35 ps was utilized for the measurements. The laser energy on the sample was measured to be (10 ± 1) mJ. The laser energy stability was determined to be 7% RMS over 200 pulses for a ramp of 25 amplifications from <0.2 mJ to 30 mJ. The initial, collimated 12 mm wide laser beam was guided towards the vacuum chamber using coated mirrors. The spot size was chosen by moving a 500 mm lens in the beam line right in front of the chamber to shift the focal point away from the sample. The craters were visually verified to be between 600 µm and 700 µm in diameter, plus an almost uniform edge of 50 µm and around 3 µm in depth, using a combination of CCD camera, confocal microscope, profilometer, and scanning electron microscope (SEM) measurements. A sample image of a crater and its characterization measured with a confocal microscope is shown in Fig. 3.

Table 1
Sample list with pre-damage, D decoration and outgassing temperature. The atomic percentage is taken from NRA and averaged over the first 1.2 µm.

Sample	damaged	D decoration	$T_{outgassing}$	D[*at*%]
I	–	Yes	–	0.08
II	Yes	Yes	902 K	0.01
III	Yes	Yes	800 K	0.20
IV	Yes	Yes	655 K	0.79
V	Yes	Yes	–	1.48
VI	Yes	Yes	629 K	0.87
VII	Yes	Yes	663 K	0.66
VIII	Yes	Yes	727 K	0.47

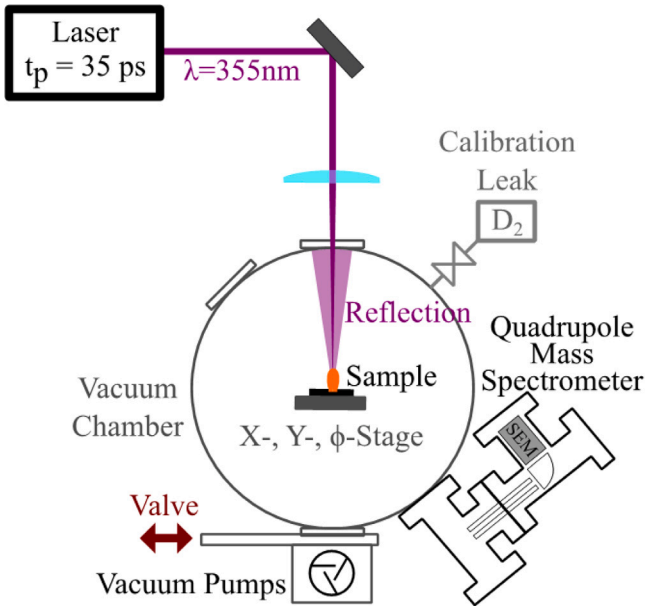

Fig. 2. Schematic experimental setup of the LIA-QMS system reduced to the key elements: the laser, the beam path, the sample holder, the quadrupole mass spectrometer, the turbo molecular pump with isolation valve, and calibration leak path. [16].

2.3. Calibration of the QMS

Before measuring the deuterium content, the QMS was calibrated to enable quantification. The calibration procedure involved the following steps: the calibration leaks were closed, and the background signal was obtained by isolating the pump for 20 s. Afterwards, the procedure was repeated with both calibration gases (H_2 and D_2) by opening the corresponding valve, with 15 min of pumping before opening the other valve to clean the pipe between the leaks and towards the chamber. The background-subtracted slope of the QMS signal represents a measure of the atoms per QMS signal unit (atoms/A). In the end, the calibration factor, C_f, was calculated after the experiments using the slope (S_{lin}) of the signal increase, determined by both linear and quadratic fit functions as a cross-check. The calibration factor is defined as:

$$C_f = \frac{S_{lin}}{L * k_b T} \quad (1)$$

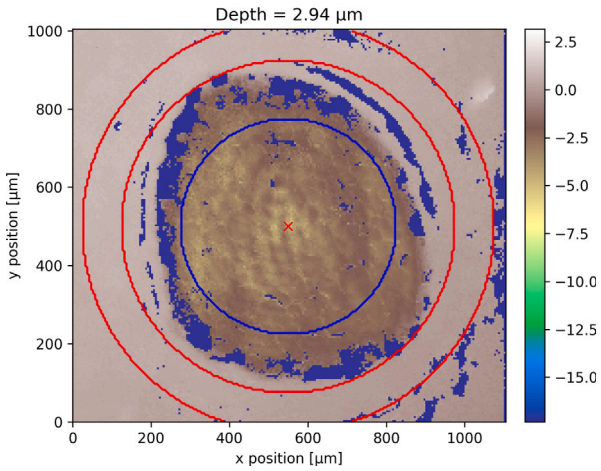

Fig. 3. Height map of a crater on sample VII measured with a confocal microscope relative to the surface. The crater bottom has an elliptical shape, with short and long axes of around 600 µm and 700 µm, and an almost uniform edge of 50 µm. Dark blue areas lack height information, mainly along the crater edge due to steep terrain and high reflectivity. The blue circle marks the area over which the mean depth of the crater bottom was averaged. The area within the two red circles was used to calculate the mean surface height. The depth value given is the difference between the computed surface and the crater bottom. (For interpretation of the references to color in this figure legend, the reader is referred to the web version of this article.)

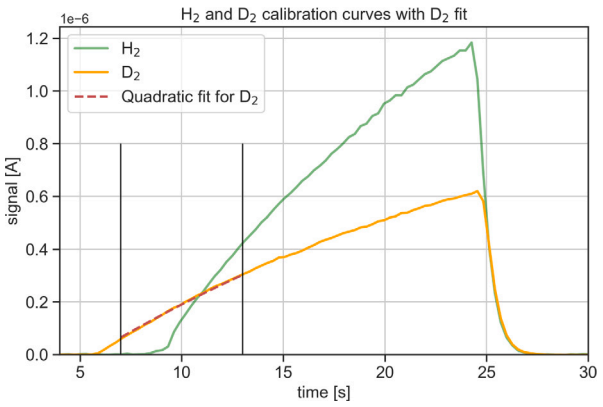

Fig. 4. Calibration curve for a 15 s calibration procedure with H_2 and 20 s for D_2 with the signal intensity on the *y*-axis and the measurement time on the *x*-axis. The black lines mark the start and end of the quadratic fit for D_2, marked in a dashed red curve. (For interpretation of the references to color in this figure legend, the reader is referred to the web version of this article.)

where L is the leakage rate, k_b is the Boltzmann constant, and T is the temperature. C_f represents the signal per molecule. Thus, division by a factor of 2 is applied to obtain the D quantity. To determine the calibration factor for HD, which was expected to be present in significant quantities along with D_2, the mean value of the calibration data from both H_2 and D_2 was used. A sample calibration curve for H_2 and D_2 is shown as an example in Fig. 4. The calibration data demonstrate a linear relationship between the QMS signal and the gas flow rate, enabling accurate quantification of the D content in this pressure range. Please note that deviations from a quadratic polynomial fit were negligible. Still, non-linear effects arising from the different orders of magnitude between the signal and calibration ranges might affect this calibration factor similarly across all samples.

2.4. LIA-QMS analysis

To determine the deuterium quantity in the LIA-QMS measurements, two separate protocols were employed for the first batch of 4 samples and the second batch of 4 samples. The difference between the two protocols was due to improvements in the valve system, which enabled faster and longer measurements after the first batch was already processed.

For the first batch, the valve to the vacuum pump was isolated 1 s before a train of 10 laser pulse salvos within 2 s. After a total of 5 s with the valve closed, it was reopened for 5 s. This procedure was repeated 20 times to achieve a maximum ablation depth of 3 µm with 150 pulses, resulting in an average ablation rate (AAR) of approximately 15 nm per pulse on W. Simultaneously, the line emission of the laser-induced plasma was recorded by the spectrometer for spectral analysis. Details about the spectrometer system and the results can be found in [18].

In contrast, the second batch of samples was analyzed with single-pulse resolution. A total of 200 pulses were fired, with a single pulse per cycle, 3 s of closing time, and 3 s of pumping time between cycles. This approach provided a 10-fold higher depth resolution compared to the first batch, while the total quantities remained unaffected. The D signal for all samples was extracted from the mass spectra at m/z = 3 ("HD") and m/z = 4 ("D_2"). The peak heights after each set of laser pulses were background-subtracted using the mass-spectrum signal during the pump-down phase and the zero measurement offset (ZMO), which is the D content measured by repeating the procedure on a non-damaged, non-D-decorated W sample. The ZMO is discussed in detail in Section 3.5. The peaks were then quantified by using the calculated calibration factor, and relative D concentrations were determined by relating the absolute content to the ablated volume. This was achieved using the standard values for W bulk material (ρ_W = 19.3 g/cm^3, M_W = 184 u) and approximating the laser crater as elliptical.

3. Results

The results of this study are structured into three sections: First, the mean D inventories determined with LIA-QMS and NRA are compared for all samples. Secondly, the D depth profiles for the batch 2 samples are analyzed in detail. Thirdly, further analyses addressing discrepancies between the results of both diagnostic techniques are provided. These include the impact of an oxide layer, the HD/D_2 ratio, and the zero measurement offset.

3.1. Comparison of the mean D content between LIA-QMS and NRA

Quantification of the D inventory inside wall material is one of the key goals of LIA-QMS. In this study, the two batches of samples were investigated using a multi-step approach: Batch 1 samples were analyzed with manual valve control. The batch 2 D inventory was determined using an automated valve. Automating the valve allowed much more detailed depth profiling, which is discussed afterwards.

3.1.1. Batch 1 D inventory comparison

The D inventory of the W samples from batch 1, determined with LIA-QMS and NRA, is shown in Fig. 5. The D inventory is averaged over 1.2 µm, matching the depth affected by damage. Using this batch, LIA-QMS was tested for its ability to detect low quantities of D and how well the detected quantity matches NRA. Sample I was undamaged, decorated with D but not outgassed which explains that NRA can detect a low amount of D of 0.08 at%. In sample II which was damaged, decorated with D but also outgassed at 902 K, NRA measures less than 0.01 at%. In contrast, LIA-QMS does not detect D in both samples after subtraction of the zero measurement offset (ZMO). The ZMO is the signal obtained on an outgassed, non-decorated sample and will be discussed in Section 3.5. The D absence in sample II is consistent with NRA and expected due to outgassing at 902 K. Samples III and IV show measurable D content in both methods. 1.8 times to 2.2 times

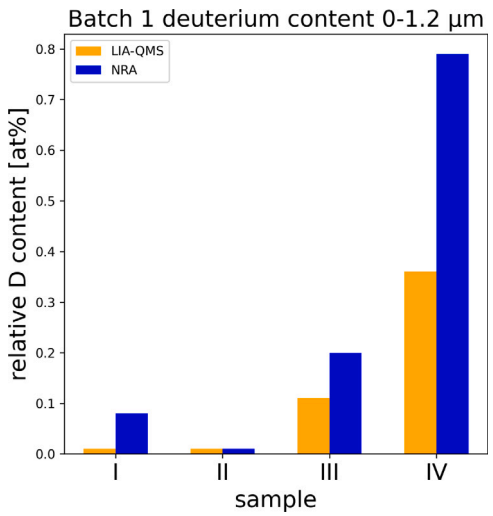

Fig. 5. Comparison of the mean D content over 1.2 µm between LIA-QMS (orange) and NRA (blue) for batch 1. Sample I was not damaged, but D was decorated, sample II, III, and IV were damaged, decorated, and outgassed at different temperatures, correlating with the remaining inventory. (For interpretation of the references to color in this figure legend, the reader is referred to the web version of this article.)

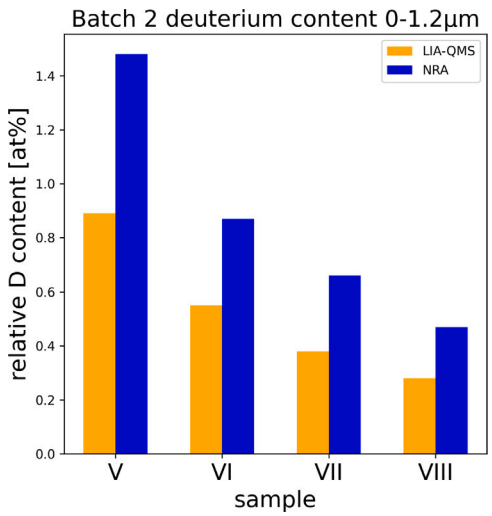

Fig. 6. Comparison of the mean D content of batch 2 over 1.2 µm between LIA-QMS (orange) and NRA (blue). (For interpretation of the references to color in this figure legend, the reader is referred to the web version of this article.)

the amount of the QMS measurements is detected via NRA. It should be noted that, due to inhomogeneities in sample IV, the uncertainty in the content is approximately 10%.

3.1.2. Batch 2 D inventory comparison

To evaluate the sensitivity and depth-profiling capability of LIA-QMS further, batch 2 was analyzed using the automated valve and up to single pulse resolution. The maximum single-pulse resolution was 15 nm AAR, given the available laser energy and a suitable crater diameter. The mean D content measured over 1.2 µm with LIA-QMS and NRA can be compared in Fig. 6. First, all samples show a similar trend: smaller D inventory at higher outgassing temperatures, which matches the findings of the batch 1 measurements and creates a database of 8 different D contents in total. Similar to batch 1 the quantification differs by a factor of around 1.7 with more D content found in the NRA measurements.

3.2. Depth profile comparison

The depth profile of samples V for one measurement with 15 nm AAR and one shot per LIA cycle is shown in Fig. 7 for both LIA-QMS and NRA after calibration and scaling. The pattern in which D is distributed remains the same across different samples despite differences in mean content, which is expected given the similar treatment, except for the outgassing temperature. The corresponding profiles of samples V, VI, VII, and VIII for both NRA and LIA-QMS are shown in Fig. 8(a) and Fig. 8(b). In general, both LIA-QMS and NRA match well. Beyond 700 nm, the D content decreases, and at around 1.7 µm, no D is detected with either method. At 250, 500, and 800 nm, small peaks are detected in the LIA-QMS profiles that were not resolved in the NRA measurements, which had around 150–400 nm resolution. The profiles deviate at the surface between 0 and 350 nm. In the NRA profile, a constant or increasing D content is measured, whereas in LIA-QMS, a high initial concentration with a substantial drop within the first 10 pulses is observed. Up to 6 at% are detected with the QMS on sample V, while NRA detects only 1.7 at%. Since differences in the ablation rate can cause large deviations in the detected quantity, the post-ablation surface was investigated. Unfortunately, no measurement method available was able to resolve the first 10 pulses for ablation

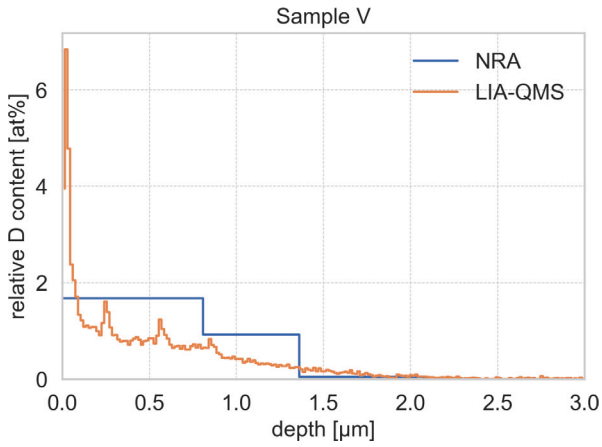

Fig. 7. LIA-QMS D depth profile (orange) compared with the first measured NRA profile (blue) on sample V, the sample of batch 2 with the highest D content. A substantial decrease in the LIA signal is noticeable in the surface region; 3 smaller peaks at 0.25, 0.5, and 0.8 µm are visible. In total, 200 cycles were carried out with 15 nm AAR. (For interpretation of the references to color in this figure legend, the reader is referred to the web version of this article.)

rate evaluation. SEM images, such as Fig. 9(a), show differences in the surface morphology within the first five pulses, which indicate changing ablation rates, but this effect is not visible afterwards, where LIA-QMS still detects a decrease of D content. The surface structure inside the crater does not undergo visible changes during the upcoming pulses; compare Figs. 9(a) and 9(b). In addition to the surface structure, the oxygen content in the craters was measured with EDX to indicate W oxide layers and hence different ablation rates, which are compared in the following.

3.3. Surface analysis of the oxygen concentration

To study the impact of potential oxygen contamination at the surface on the ablation rates and fuel content, dedicated craters were analyzed as shown in Fig. 9(a). An increased oxygen content would indicate the presence of WO layers, which would lead to different ablation rates in comparison with bulk W, since LIA methods tend to

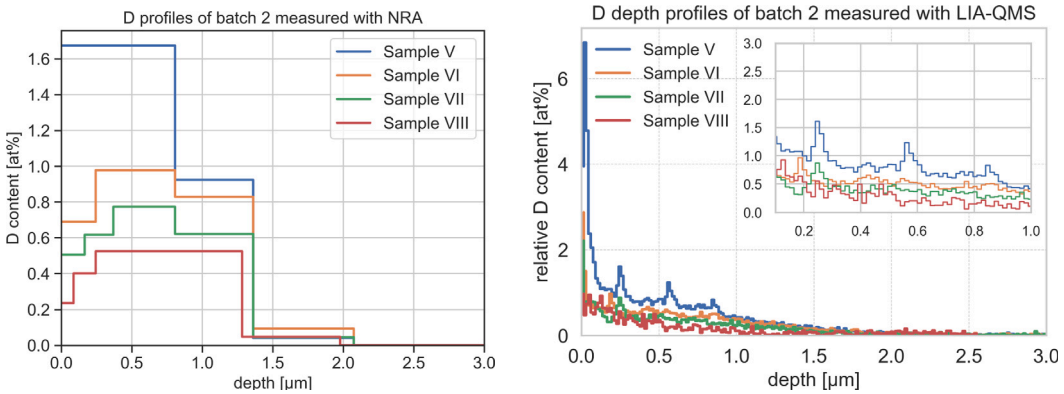

Fig. 8. D depth profiles of batch 2 for NRA (a) and LIA-QMS (b) after calibration of the LIA-QMS signal. With NRA, an initial rise in D concentration is observed within the first 300 nm, while a substantial decrease is observed with LIA-QMS. All samples show the same trend but with differing mean concentrations. 3 peaks are detected with LIA-QMS at 250, 500, and 800 nm in samples V, VI, and VII.

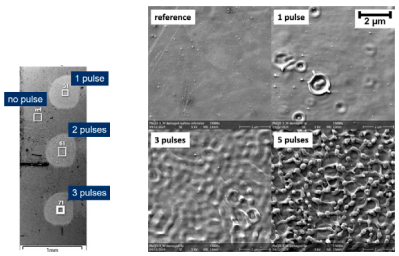

Fig. 9. (a) SEM image of the three reference craters after the first, the second and third laser pulse at 20 mJ laser energy. The reference point for the oxidation concentration comparisons is marked, assuming comparable initial surface conditions before laser impact. (b) Comparison of the surface structure of the W sample III, all with magnification 15000x.

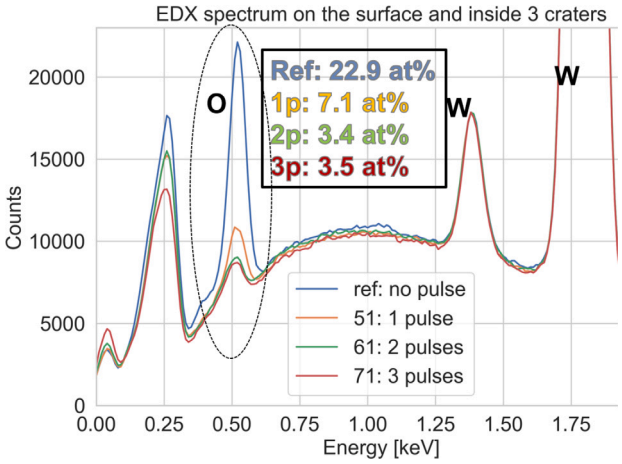

Fig. 10. EDX spectrum of all four marked points in Fig. 9(a) including a carbon peak at 0.25 keV, an oxygen peak at 0.5 keV, and two W peaks at 1.35 KeV and 1.8 keV. The strong oxygen signal drops rapidly between the reference point and the first laser pulse, decreases towards the second pulse, and remains nearly the same concentration at the third pulse.

remove layers with different compositions at different rates. Independent surface composition analysis with respect to the laser methods and evaluation of the impact of O was done using EDX, as shown in Fig. 10. Between the reference point, an unperturbed area on the sample indicated in Fig. 9(a), and the first laser pulse, the difference in O content is the largest with ~16%, decreasing to ~4% between the first and second laser pulse and vanishing between the second and third laser pulse without a significant difference. The drop in O content within two pulses indicates a compositional change and the removal of a very thin oxidized layer at the top surface. The negligible amount of O and its constancy after the two pulses indicate that the possible impact of an oxidized layer on the fuel content is limited to the first two pulses and thus does not explain the substantial decrease in concentration over the first 10 pulses. Complementary to the EDX findings, the calculation of the O concentration for μ-NRA, performed simultaneously with the D measurement, indicates a decrease in O concentration after laser ablation.

3.4. HD and D_2 ratio

Besides the depth profiles themselves, the ratio between HD and D_2 was analyzed to understand possible recombination processes at the chamber's wall, which contain even after conditioning residual amounts of hydrogen at the surface. Fig. 11 highlights the different profiles for HD and D_2 on sample V, which contain a higher deuterium content than the others. While atomic deuterium is expected in the W sample, it certainly recombines during interactions inside the laser-induced plasma or with the chamber's wall. The D content ratio between HD and D_2 shows a lot more HD than D_2. The shape of the D distribution is similar in both, but does not correlate entirely. While the D_2/HD ratio at the surface-near region is 1:1, deeper inside the D_2 ratio decreases to only 1:3 (450–600 nm) and 1:5 (900–1050 nm). In addition to the D_2 to HD ratio, the H_2 profile is shown in Fig. 11 to evaluate possible correlations of the three peaks in the D profiles with naturally abundant HD in hydrogen molecules. The H_2 profile shows an increase in signal with depth, which might be caused by a slight increase in chamber pressure over the long measurement duration and the short pumping time between cycles. Nevertheless, the profile cannot explain the peaks appearing in both the HD and D_2 profiles.

3.5. Zero measurement offset

The interactions with the chamber's wall are not only determined by the recombination post laser ablation and fuel release, but they are also determined by the surprisingly high HD content in non-D-decorated but also D-decorated samples. Fig. 12 compares the H_2 and HD signal on an annealed reference sample (1 h at 1300 K) without damage and

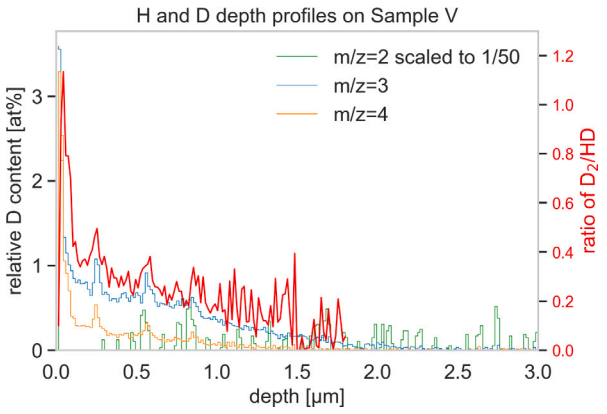

Fig. 11. Comparison of m/z = 2 (H_2), m/z = 3 (HD), m/z = 4 (D_2) and content for sample V. The ratio between D_2 and HD decreases strongly with depth, showing a large peak at m/z = 4 in the first pulses. The H_2 profile does not correlate with the three peaks visible in mass 3 and 4.

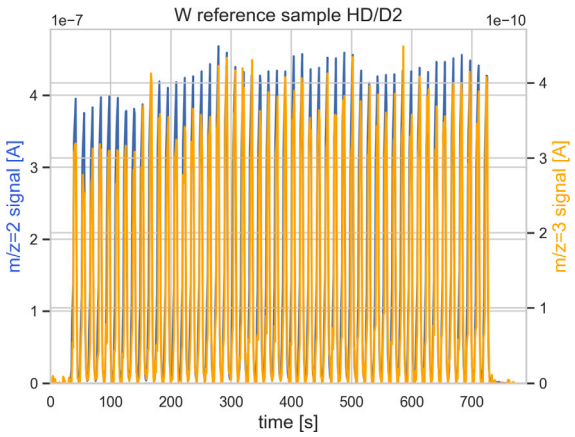

Fig. 12. H_2 QMS signal in blue compared with the HD signal in orange over 50 cycles with one pulse on a non-damaged and non-decorated reference sample. Two *y* axes were used to compare the time-resolved patterns, the left one for H_2, the right one for HD. (For interpretation of the references to color in this figure legend, the reader is referred to the web version of this article.)

deuterium decoration. It is noticeable that the HD content is ~0.1% related to H_2, which is about 10 times higher than the natural abundance of 0.015%. Besides that, the graph shows a correlation between HD and H_2 signal, which would also represent the main contribution to the background of D-decorated samples. Nevertheless, there is a slight difference in the background HD signal between non-damaged W, non-decorated W, and decorated W. The D content in decorated W is higher, most likely driven by the small amount of ablation of more superficial layers at the crater edge, where the ablation rate is lower due to lower fluence. The μ-NRA measurements also indicate a remaining fraction of D in the crater edge, which represents ~17% of the crater. A complex deconvolution of the signal for each laser pulse has been excluded due to the large ratio between the crater bottom and edge. Still, it should be considered in studies of maximum sensitivity and deeper craters, with a changing aspect ratio. Especially in the superficial region, the influence of the crater edge can lead to an overestimated amount of D or an underestimated ablated area, also indicating a higher D at the surface than in the NRA measurements. A μ-NRA crater map on sample VII is shown in Fig. 13; the maps of the other craters look similar. The independent NRA method confirms that LIA-QMS removes all D out of the crater center with a steep and almost uniform edge of around 50 µm. The thermal influence at the sides appears very limited and negligible for the crater diameters applied here, at a minimum. 500 µm. The edge width can be determined by the flat-top laser beam profile, which causes less ablation at the edge and leaves part of the D-containing layer.

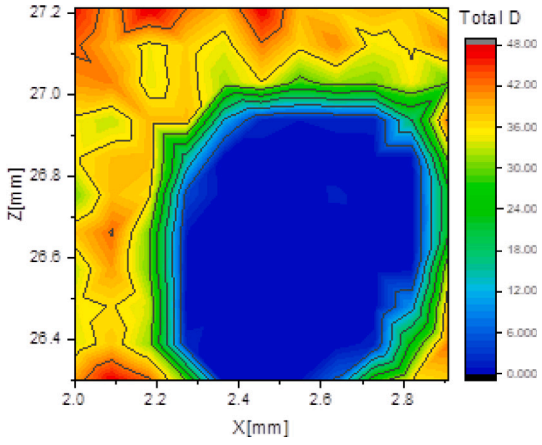

Fig. 13. μ-NRA map of the D content on sample VII. Red to orange color represents the original D content where no LIA crater was created. Green color marks the 50 µm wide edge of the crater with a fraction of D remaining, and blue the 600 µm wide center with no D remaining. (For interpretation of the references to color in this figure legend, the reader is referred to the web version of this article.)

4. Discussion

As demonstrated, ps-LIA-QMS can provide highly resolved and sensitive H isotope depth profiles in absolute concentrations. However, the results presented above reveal additional requirements in the analysis procedure and uncertainties. Notably, the quantification requires a precise calibration setup and knowledge about the crater parameters, such as the depth, crater edge, and crater bottom area. Deviations in surface area have a significant impact on the calculated D content. They must be prevented by creating crater databases for different materials and laser parameters using ex-situ diagnostics, such as confocal microscopy, or by adding supplemental in-situ diagnostics later on. Regarding the consistently differing mean quantity of detected D relative to NRA by a factor of 1.7, multiple contributors could play a role. A potential cause of D signal loss was observed during implantation in the chamber wall, specifically in the glass window facing the sample, which is the primary target for ablated material. The 35 ps laser beam releases high-energy atoms from the target's surface during the ablation process [18], which could potentially be implanted inside the chamber wall and remain undetectable. Studies with femtosecond lasers have reported even more significant losses of up to 97% [22]. Although this loss can be corrected using a reference sample with known D content, it is crucial to understand this aspect for reliable operation in a fusion reactor, given the changing properties of interacting surfaces. Variations in distance to the target, incident angles of ablated material, and compositions may affect the signal. Therefore, incorporating a predefined first interaction area into the diagnostic setup may be necessary. Another possibility is the influence of the crater edge and local changes of the ablation rate to the depth localization of D. If some regions show a lower ablation rate. The D is seen in deeper layers, interfering with the contribution of the crater edge to deeply measured D. To clarify this in the future, areal densities could be determined after deeper measurements that also ablate most of the D-containing crater edge. Furthermore, the chemistry during the ionization and mass analysis within the QMS might cause pressure-dependent isotope exchange, leading to non-linearities. These could affect the calibration factor for H_2 and, mainly, D_2 by contributing to the HD signal. Analyses using a smaller calibration leak are required to

validate this point. Regarding the D_2 to HD ratios, molecular recombinations on the sample or on the wall could explain the higher detection of HD compared to D_2. Furthermore, the significantly higher presence of H compared to D increases the HD to D_2 recombination ratio in the chamber.

The relatively constant, but high ZMO of H_2 and HD, even when the sample is not damaged or loaded, strongly suggests isotope exchange and recombination. Another possibility is the desorption of surface water and H isotopes, which builds up between the cycles. Indications for the amount were found with simultaneous LIBS measurements showing a strong increase of the H signal in each first pulse of an LIA cycle after opening and closing the valve to the chamber. These findings are discussed further in a future publication. Although the HD content is 10 times higher than the natural abundance of HD in hydrogen molecules, this can be due to two factors: the experimental setup using D in the samples and the calibration influx, and isotope exchange in the mass spectrometer. The difference in background signal between non-loaded and loaded samples is likely caused by D emitted from the crater edge, where the ablation rate is lower. For the craters of the aspect ratio presented this effect is negligible. For craters with smaller aspect ratios (radius/depth) and depths greater than 10 μm, this deviation may change; this should be considered in future studies. Comparing the characteristics of QMS-measured profiles and NRA, the most significant difference is observed in the first ~20 laser pulses, where QMS measures a higher D content than NRA. Previous studies on the same samples using LIBS showed similar effects [18]. This suggests that the cause lies in the ablation process. One possibility is a differing ablation rate over the first 20 pulses, as the AAR has a proportional influence on D content. However, SEM images of the crater structure indicate that such a change is unlikely. Other available methods were unable to reliably determine the ablation rate after only a few pulses, so the structure and EDX measurements are the only data available here. EDX analysis also revealed significant oxidation on the samples, but the oxide layer was ablated after 2–3 pulses, leaving no noticeable residue. To gain insight into the deviations more superficial than 300 nm, ultra-high-resolution crater analyses in the order of 10 nm would be necessary for validation. The second possibility is the crater edge, whose formation could reduce the ablated area due to the decreasing incident angle of the beam on the edge. Deconvolution for this theory is ongoing. A third possibility that could affect the superficial region is thermal influence from the picosecond laser. As we are above the non-thermal ablation threshold of approximately 1 ps, thermal effects are expected. Thermal effects should mostly be visible in the QMS profiles, but not in LIBS, since LIBS requires plasma formation, which is much less likely when particles come from deep inside the material. Nevertheless, it cannot be excluded that the extremely high temperatures at the W surface are still sufficient to release the particles from deeper regions. Time resolved simulations of the D diffusion and trap annealing after ps laser irradiation are currently developed on to understand the QMS and LIBS profiles further.

Examining the depth profile in more detail, D content and distribution align well with NRA results after quantification and normalization, providing an even more detailed profiling than NRA revealing three smaller peaks at 0.3, 0.5, and 0.7 μm in sample batch 2. These peaks are only visible in the HD and D_2 signal but also in LIBS profiles. Their appearance in all samples of batch 2 with decreasing total content cannot be explained by the typical damage type and density distribution in self-damaged W [23,24]. Regarding batch 1, sample IV could have shown these peaks too, but due to the low resolution with which these measurements have been done, and TDS measurements done afterwards, this cannot be checked anymore. Fluctuations during the measurement, such as changing room temperature or focus, can be excluded since the temperature is permanently controlled and the peaks would appear in different positions and not so consistent at certain depths. The release of D at grain boundaries can be excluded in these samples, since the grains are much larger than 300 nm. A possible reason for the peaks might be the ablation of surface structures, such as W micropillars that build up at certain fluences. Since the peaks appear approximately at depths multiple times the laser wavelength, interference and a higher ablation probability at these depths cannot be excluded and require further investigation. The peaks do not negatively impact the study; instead, they provide additional reference points that prove the reproducibility of the experiments and high-resolution similarities between LIBS and LIA-QMS.

5. Summary and conclusion

In total, our findings demonstrate that the use of picosecond lasers for LIA-QMS yields high-resolution D depth profiles with a comparably high penetration depth in 4 μm range, primarily limited by structures formed on the bottom of the craters causing roughness in the current setup. The thermal effects of the picosecond laser appear to have a significant impact on the surface region, but a minor impact on large scales, leading to an overestimated concentration at the surface and a slight shift of the D towards the surface. Characteristic features such as the rapid fall-off or the end of the D decoration can be accurately determined using this method. The D content, compared to the reference, can be reproduced using a scaling factor of 1.7. With an average ablation rate of 15 nm, ps-LIA-QMS is competitive with LIBS and NRA in depth resolution and, especially compared to NRA, offers a simpler setup without an accelerator, making it suitable for in-situ studies. Combining simultaneous LIBS and LIA-QMS measurements seems to be a practical approach to optimize diagnostic versatility and independently validate the acquired profiles, which will be explored in future studies. Although LIA-QMS exhibits promising depth profiling capabilities for future fusion reactors, specific findings, such as the significant m/z = 3 HD ZMO when ablating material, the constant deviation from the NRA quantity and the thermal effects, necessitate further investigation to ensure reliable and versatile in-situ application under diverse conditions. In terms of detection limits, ps-LIA-QMS already demonstrates sufficient sensitivity, which can be further enhanced by optimizing ZMO analysis. In conclusion, ps-LIA-QMS provides quantified, well-reproducible, high-resolution, and sensitive depth profiles in a compact setup.

CRediT authorship contribution statement

C. Kawan: Writing – review & editing, Writing – original draft, Visualization, Project administration, Methodology, Investigation, Formal analysis, Data curation, Conceptualization. **S. Brezinsek:** Supervision, Project administration, Methodology, Funding acquisition, Conceptualization. **E. Wüst:** Writing – review & editing, Methodology, Investigation, Formal analysis, Data curation, Conceptualization. **T. Dittmar:** Writing – review & editing, Supervision, Investigation, Conceptualization. **T. Schwarz-Selinger:** Writing – review & editing, Validation, Investigation, Formal analysis. **M. Rasinski:** Writing – review & editing, Resources, Investigation, Formal analysis. **S. Möller:** Writing – review & editing, Visualization, Resources, Methodology, Investigation, Formal analysis. **L. Gao:** Project administration. **Ch. Linsmeier:** Supervision, Project administration, Funding acquisition.

Declaration of Generative AI and AI-assisted technologies in the writing process

During the preparation of this work the authors used generative AI of Grammarly Inc. in order to improve the manuscript's readability. After using this tool, the authors reviewed and edited the content as needed and take full responsibility for the content of the publication.

Declaration of competing interest

The authors declare that they have no known competing financial interests or personal relationships that could have appeared to influence the work reported in this paper.

Acknowledgments

This work has been carried out within the framework of the EUROfusion Consortium, funded by the European Union via the Euratom Research and Training Programme (Grant Agreement No 101052200 — EUROfusion). However, views and opinions expressed are those of the author(s) only and do not necessarily reflect those of the European Union or the European Commission. Neither the European Union nor the European Commission can be held responsible for them.

Funded by the Deutsche Forschungsgemeinschaft (DFG, German Research Foundation), Germany – 491111487.

References

[1] P.H. Rebut, R.J. Bickerton, B.E. Keen, The joint European torus: installation, first results and prospects, Nucl. Fusion 25 (9) (1985) 1011–1022.

[2] A. Loarte, R.A. Pitts, T. Wauters, I. Nunes, P. de Vries, S.H. Kim, F. Köchl, A. Polevoi, M. Lehnen, J. Artola, S. Jachmich, A. Pshenov, X. Bai, I.S. Carvalho, M. Dubrov, Y. Gribov, M. Schneider, L. Zabeo, X. Bonnin, S.D. Pinches, F. Poli, G. Suarez Lopez, M. Merola, F. Escourbiac, R. Hunt, L. Chen, D. Boilson, P. Veltri, N. Casal, M. Preynas, A. Mukherjee, W. Helou, F. Kazarian, S. Willms, I. Bonnet, R. Michling, L. Giancarli, J. van der Laan, M. Walsh, V. Udintsev, R. Reichle, G. Vayakis, A. Fossen, M. Turnyanskiy, A. Becoulet, Y. Kamada, G. Zhuang, G. Xu, X. Gong, J. Huang, M. Jia, R. Ding, J. Qian, Y. Sun, Q. Yang, L. Zhang, M. Xu, S. Brezinsek, J. Stober, J. Hobirk, F. Rimini, J. Garcia, S.L. Rao, J. Ghosh, D. Sharma, B. Magesh, R.P. Bhattacharya, G. Matsunaga, H. Urano, T. Hirose, K. Ogawa, G. Motojima, C.K. Sung, H.H. Lee, J.K. Park, M.S. Cheon, Y.M. Jeon, S. Konovalov, S. Lebedev, N. Kirneva, Y. Kashchuk, N. Bakharev, X. Chen, A. Bortolon, L. Casali, R. Maingi, F. Turco, K. Schmid, Y. Liu, J.R. Martín-Solís, C. Angioni, I. Pusztai, D. Fajardo, D. Mateev, E. Lerche, D. van Eester, P. Vincenzi, R. Futtersack, V. Bobkov, L. Colas, The new ITER baseline, research plan and open R&D issues, Plasma Phys. Control. Fusion 67 (6) (2025) 065023.

[3] Yong-Gang Li, Qi-Rong Zheng, Liu-Ming Wei, Chuan-Guo Zhang, Zhi Zeng, A review of surface damage/microstructures and their effects on hydrogen/helium retention in tungsten, Tungsten 2 (1) (2020) 34–71.

[4] James Dark, Rémi Delaporte-Mathurin, Thomas Schwarz-Selinger, Etienne A. Hodille, Jonathan Mougenot, Yann Charles, Christian Grisolia, Modelling neutron damage effects on tritium transport in tungsten, Nucl. Fusion 64 (8) (2024) 086026.

[5] Michael Rieth, Russell Doerner, Akira Hasegawa, Yoshio Ueda, Marius Wirtz, Behavior of tungsten under irradiation and plasma interaction, J. Nucl. Mater. 519 (2019) 334–368.

[6] R. Rayaprolu, S. Möller, R. Abernethy, M. Rasinski, J.C. Haley, Ch. Linsmeier, Indentation testing on 3 MeV proton irradiated tungsten, Nucl. Mater. Energy 25 (2020) 100776.

[7] I. Ipatova, R.W. Harrison, P.T. Wady, S.M. Shubeita, D. Terentyev, S.E. Donnelly, E. Jimenez-Melero, Structural defect accumulation in tungsten and tungsten-5wt.% tantalum under incremental proton damage, J. Nucl. Mater. 501 (2018) 329–335.

[8] T. Schwarz-Selinger, Deuterium retention in MeV self-implanted tungsten: Influence of damaging dose rate, Nucl. Mater. Energy 12 (2017) 683–688.

[9] Yong Wu, Predrag Krstic, Fu Yang Zhou, Fred Meyer, Damage at a tungsten surface induced by impacts of self-atoms, J. Nucl. Mater. 467 (2015) 480–487.

[10] S. Markelj, M. Payet, E. Bernard, M. Lipoglavšek, M. Kelemen, A. Cvetinović, C. Grisolia, P. Pelicon, Tritium measurements by nuclear reaction analysis using 3he beam in the energy range between 0.7 MeV and 5.1 MeV, Nucl. Mater. Energy 28 (2021) 101057.

[11] M. Zlobinski, G. Sergienko, I. Jepu, C. Rowley, A. Widdowson, R. Ellis, D. Kos, I. Coffey, M. Fortune, D. Kinna, M. Beldishevski, A. Krimmer, H.T. Lambertz, A. Terra, A. Huber, S. Brezinsek, T. Dittmar, M. Flebbe, R. Yi, R. Rayaprolu, J. Figueiredo, P. Blatchford, S. Silburn, E. Tsitrone, E. Joffrin, K. Krieger, Y. Corre, A. Hakola, J. Likonen, First results of laser-induced desorption - quadrupole mass spectrometry (LID-qms) at JET, Nucl. Fusion 64 (8) (2024) 086031.

[12] A. Huber, B. Schweer, V. Philipps, N. Gierse, M. Zlobinski, S. Brezinsek, W. Biel, V. Kotov, R. Leyte-Gonzales, Ph. Mertens, U. Samm, Development of laser-based diagnostics for surface characterisation of wall components in fusion devices, Fusion Eng. Des. 86 (6–8) (2011) 1336–1340.

[13] J. Karhunen, A. Hakola, J. Likonen, A. Lissovski, M. Laan, P. Paris, Applicability of LIBS for in situ monitoring of deposition and retention on the ITER-like wall of JET – comparison to SIMS, J. Nucl. Mater. 463 (2015) 931–935.

[14] J. Likonen, S. Almaviva, R. Rayaprolu, R. Yi, I. Jepu, G. Sergienko, A. Widdowson, N. Jones, S. Atikukke, T. Dittmar, J. Karhunen, P. Gasior, Ch. Kawan, M. Sackers, S. Soni, E. Wüst, S. Brezinsek, J. Butikova, W. Gromelski, A. Hakola, I. Jõgi, P. Paris, J. Ristkok, P. Veis, First demonstration of laser induced breakdown spectroscopy using remote handling for in-vessel analysis of JET components, Nucl. Mater. Energy 45 (2025) 102021.

[15] Jannis Oelmann, Quantitative untersuchung des laserablationsprozesses mittels kombination von optischer spektroskopie und massenspektrometrie, 2019.

[16] Jannis Oelmann, Cong Li, Sebastijan Brezinsek, Marcin Rasinski, Chandra Prakash Dhard, Ralf König, Victoria Winters, Christian Linsmeier, Depth resolved analysis of hydrogen in W7-x graphite components using laser-induced ablation-quadrupole mass spectrometry (LIA-qms), Nucl. Mater. Energy 18 (2019) 153–158, URL https://www.sciencedirect.com/science/article/pii/S2352179118301893.

[17] Dongye Zhao, Ding Wu, Jannis Oelmann, Sebastijan Brezinsek, Qingmei Xiao, Rongxing Yi, Laizhong Cai, Hongbin Ding, Highly depth-resolved characterization of fusion-related tungsten material based on picosecond laser-induced breakdown spectroscopy, J. Anal. At. Spectrom. 35 (12) (2020) 2867–2879.

[18] E. Wüst, T. Schwarz-Selinger, C. Kawan, L. Gao, S. Brezinsek, Depth-resolved deuterium retention analysis in displacement-damaged tungsten using laser-induced breakdown spectroscopy, Phys. Plasmas 31 (8) (2024).

[19] K. Schmid, V. Rieger, A. Manhard, Comparison of hydrogen retention in w and w/ta alloys, J. Nucl. Mater. 426 (1–3) (2012) 247–253.

[20] M. Mayer, SIMNRA, a simulation program for the analysis of NRA, RBS and ERDA, in: AIP Conference Proceedings, AIP, 1999, pp. 541–544.

[21] B. Wielunska, M. Mayer, T. Schwarz-Selinger, U. von Toussaint, J. Bauer, Cross section data for the d(3he,p)4he nuclear reaction from 0.25 to 6 MeV, Nucl. Instrum. Methods Phys. Res. Sect. B: Beam Interactions Mater. Atoms 371 (2016) 41–45.

[22] Steffen Mittelmann, Matej Mayer, Udo von Toussaint, Benedikt Buchner, Andreas Theodorou, Thomas Dürbeck, Wolfgang Jacob, Thomas Schwarz-Selinger, Femtosecond laser-induced ablation – quadrupole mass spectroscopy (fs-lia-qms) experiment for the detection of trapped hydrogen-isotopes and helium in nuclear fusion relevant materials, 2025, http://dx.doi.org/10.2139/ssrn.5143731.

[23] Ł. Ciupiński, O.V. Ogorodnikova, T. Płociński, M. Andrzejczuk, M. Rasiński, M. Mayer, K.J. Kurzydłowski, TEM observations of radiation damage in tungsten irradiated by 20MeV w ions, Nucl. Instrum. Methods Phys. Res. Sect. B: Beam Interactions Mater. Atoms 317 (2013) 159–164.

[24] W. Chrominski, L. Ciupinski, P. Bazarnik, S. Markelj, T. Schwarz-Selinger, TEM investigation of the influence of dose rate on radiation damage and deuterium retention in tungsten, Mater. Charact. 154 (2019) 1–6.